INTERNATIONAL JOURNAL FOR NUMERICAL METHODS IN FLUIDS, VOL. 26, 101–121 (1998)

# ON RIEMANN-PROBLEM-BASED METHODS FOR DETONATIONS IN SOLID ENERGETIC MATERIALS

RICHARD SAUREL* AND JACQUES MASSONI

*IUSTI, UMR CNRS 6595, Technopôle de Château Gombert, 5 Rue Enrico Fermi, 13453 Marseille Cedex 13, France*

SUMMARY

This paper compares several high-resolution schemes for the computation of detonation waves in solid explosives. The essential difficulty in comparison with the usual application domain of these schemes is due to the complexity and variety of the equations of state which are used. The HLLC Riemann solver is used in the context of an Eulerian MUSCL scheme and in conjunction with a shock-tracking scheme. The motivation and justification for the various choices in the building of these schemes are discussed. The accuracy of both schemes, full Eulerian and shock-tracking variant, is clearly demonstrated. In addition, the validity of the results is shown. For one-dimensional applications the shock-tracking scheme is very accurate and relatively simple. For multidimensional applications it is recommended that the full Eulerian version be used. © 1998 John Wiley & Sons, Ltd.

*Int. J. Numer. Meth. Fluids*, **26**: 101–121 (1998)

KEY WORDS: Riemann solvers; Eulerian schemes; detonations; shock tracking

## 1. INTRODUCTION

During the last two decades, considerable progress has been made in the solution of the equations of gas dynamics. This progress is due to various advances in the understanding of hyperbolic systems such as the Euler equations. Riemann-problem-based methods such as second- or higher-order Godunov schemes[1] constitute very efficient tools for gas dynamics numerical simulations. The fundamental ideas of these extensions are essentially due to van Leer[2] and Roe.[3] Currently these methods are widely used in aerodynamics and offer many advantages for capturing discontinuities, especially in unsteady regimes. Gradually, these methods were extended to physical models more complicated than the Euler equations. For example, two-phase flows[4,5] as well as multispecies reactive flows[6] have been solved with this method. Their accuracy and appeal have led some researchers to apply them to more marginal hyperbolic (shallow water equations)[7] and non-hyperbolic (incompressible Navier–Stokes equations)[7] systems. Remaining in the more classical field of gas dynamics, one can notice that these methods are generally employed for ideal gas flows or ideal gaseous mixtures. Indeed, these methods have had only a few applications where the algebraic form of the equation of state differs clearly from that for an ideal gas. The main reason resides in the

Correspondence to: R. Saurel, IUSTI, UMR CNRS 6595, Technopôle de Château Gombert, 5 Rue Enrico Fermi, 13453 Marseille Cedex 13, France. Email: richard@iusti.univ-mrs.fr
Contract grant sponsor: DGA/DRET/ETCA/CEGz

CCC 0271–2091/98/010101–21 $17.50

*Received July 1996*
*Revised March 1997*

fact that the Riemann problem and the general construction of a second-order Godunov-type scheme are made considerably complicated by using a complex equation of state. This is why these methods are not used at present in the numerous detonation codes. Detonations in solid high explosives produce heterogeneous or gaseous mixtures at pressures of several hundred thousand atmospheres, inevitably governed by real gas equations of state. Classical detonation codes generally use schemes based on Taylor expansions, e.g. the central schemes of Lax and Wendroff,[8] Richtmeyer and Morton[9] and MacCormack.[10] Indeed, these schemes do not use the Riemann problem solution. For evident reasons of accuracy it would be interesting to take advantage of the Riemann-based methods for the calculation of detonation waves. This cannot be realized without a careful analysis, because it is necessary, apart from the usual qualities required of a numerical method (accuracy, stability, convergence), to fulfil also qualities of robustness, rapidity and flexibility with model modifications. This last characteristic is of uppermost importance. Indeed, for the simulation of modern detonation problems it is important to be able to add or subtract easily some 'species equations' to or from the model. This type of modification of the system of equations has to be easily compatible with the method used to solve the equations. It is also very important to be able to change easily the equations of state, knowing that they can be expressed in various algebraic forms. For their adaptation in the method these equations of state should not introduce an increase in computational time and prohibitive algebraic calculations. Strictly speaking, the present work does not contain a new method. Here, various possibilities for the construction of a high-resolution scheme satisfying the previously mentioned criteria are examined. One proposes therefore a management with various ingredients, taking care to motivate and justify the retained choice. The final method proposed here is Eulerian and is a second-order Godunov-type scheme. A shock-tracking variant of this scheme is proposed and detailed. This extension is important for some applications in which shock wave numerical diffusion is not admissible.

## 2. THE MODEL

The model presented here is very representative of problems solved in modern detonation codes. It consists of the Euler equations coupled with a certain number of species equations to track the kinetics of explosive decomposition. Modern detonation problems are rarely reduced to kinetic decomposition models with an unique variable. The equation of state used in this study is a function of three variables. It is nevertheless usual to see equations of state as a function of two variables only (pressure depends on density and internal energy): $P = P(\rho, e)$ or $e = e(\rho, P)$. These equations of state are adapted only to a reduced number of detonation problems and exclude in all cases an accurate resolution of the reaction zone within the detonation wave. We adopt a formulation $P = P(\rho, e, \lambda)$ or $e = e(\rho, P, \lambda)$, where $\lambda$ is the global advancement parameter of the decomposition reactions. This choice for the equation of state complicates the numerical algorithm because it restricts our choice for the real gas Riemann solver, since only a few such solvers apply to equations of state containing more than two variables.

The fluid dynamics equations are expressed as the Euler equations

$$\frac{\partial \rho}{\partial t} + \frac{\partial \rho u}{\partial x} = 0, \tag{1}$$

$$\frac{\partial \rho u}{\partial t} + \frac{\partial (\rho u^2 + P)}{\partial x} = 0, \tag{2}$$

$$\frac{\partial \rho E}{\partial t} + \frac{\partial u(\rho E + P)}{\partial x} = 0, \tag{3}$$

 

where $\rho$ designates density, $u$ velocity, $P$ pressure and $E$ total energy. Total energy and internal energy used in the equation of state are related by $E = e + \frac{1}{2}u^2$. The decomposition model uses three variables. The kinetic scheme follows the work of Johnson *et al.*[11] (JTF). When a shock wave propagates into the explosive, hot spots are created locally. Decomposition of the explosive starts around these hot spots and is followed by bulk decomposition. Evolution of the global decomposition parameter is given by

$$\frac{\mathrm{d}\lambda}{\mathrm{d}t} = \mu\frac{\mathrm{d}f}{\mathrm{d}t} + (1-\mu)\frac{\mathrm{d}g}{\mathrm{d}t}, \tag{4}$$

where $f$ represents the decomposition fraction from hot spots and $\mu$ is a parameter of the kinetics. The kinetics of hot spot decomposition is written as

$$\frac{\mathrm{d}f}{\mathrm{d}t} = (1-f)Z\frac{\alpha\beta}{\theta^2}\mathrm{e}^{-\alpha/\theta}, \tag{5}$$

where $Z, \alpha$ and $\beta$ are parameters and $\theta$ represents the hot spot temperature. Note that this law of decomposition is of Arrhenius type, representative of a broad class of kinetic laws for energetic materials. Evolution of the bulk decomposition is given by $g$ and follows the equation

$$\frac{\mathrm{d}g}{\mathrm{d}t} = 0 \quad \text{if } f < f_0 \tag{6}$$

or

$$\frac{\mathrm{d}g}{\mathrm{d}t} = (1-g)\frac{f-f_0}{1-f_0}[G_0 + F(P_{\text{shock}})]\left(\frac{P}{P_0}\right)^r \quad \text{if } f > f_0, \tag{7}$$

where

$$F(P_{\text{shock}}) = A\left(\frac{P_{\text{shock}}}{P_0}\right)^{n-r}\left[1 + B\left(\frac{P_{\text{shock}}}{P_0}\right)^{7-n}\right]. \tag{8}$$

In these equations, $P_{\text{shock}}$ represents the shock pressure and $P_0, r, n, A, B$ and $f_0$ are parameters. Note that this second kinetic law is a function of pressure to the power of a certain exponent and is representative of the second main class of kinetic laws for energetic materials (Vieille-type laws). This kinetics necessitates a closure law for the hot spot temperature. It is expressed by the empirical formulation

$$\theta = \theta_0 \exp\left(\frac{\Gamma_k(P - P_{\text{shock}})}{1 - m(\theta_0/\alpha)\ln(P_{\text{shock}}/P_0)}\right), \tag{9}$$

where $\theta_0, \Gamma_k$ and $m$ are constant parameters. Equation (9) is a function of pressure immediately behind the shock wave, inside a control volume (mesh). Time evolution of the shock pressure is given by

$$\frac{\mathrm{d}P_{\text{shock}}}{\mathrm{d}t} = 0, \tag{10}$$

valid after shock wave passage.

The operator $\mathrm{d}/\mathrm{d}t$ present in equations (4)–(7) and (10) represents the convective derivative $\mathrm{d}/\mathrm{d}t = \partial/\partial t + u\partial/\partial x$. The complete equation system necessitates for its closure an equation of state. A detonation in a solid (or gaseous) explosive consists of a shock wave followed by rapid decomposition of the solid reactant to form gaseous products (ZND model). Therefore it is necessary to have a representative equation of state for the two-phase solid–gas flowing mixture. A possible

 

formulation is that proposed by Baudin and Bergues.[12] In this formulation the gaseous phase is represented by the JWL equation of state[13] widely used in detonation, while the solid is governed by the Cochran and Chan[14] (CC) equation of state. These equations of state are based on two assumptions: constant values for the specific heat capacity at constant volume ($C_v$) and Gruneisen coefficient ($\Gamma$). These equations of state can be written in Mie–Gruneisen algebraic form. By combination of these two equations of state and with the help of the pressure equilibrium assumption between the two phases one obtains a Mie–Gruneisen-type mixture equation of state

$$e(P, \rho, \lambda) = e_k(\rho, \lambda) + \frac{P - P_k(\rho, \lambda)}{\rho\Gamma(\lambda)}. \tag{11}$$

The various functions appearing in this equation are given in the Appendix. Furthermore, since the numerical strategy is based on the Riemann problem resolution, it is necessary to know the sound speed:

$$c^2 = \frac{P - \rho^2(\partial e/\partial\rho)_{P,\lambda}}{\rho^2(\partial e/\partial P)_{\rho,\lambda}}. \tag{12}$$

Partial derivatives appearing in the equation of state are also given in the Appendix. Convexity of the equation of state (11) has been demonstrated.[12] This is an important property for the Riemann problem solution. As the full set of equations has to be solved by a Eulerian method, it is preferable to write it in conservative form, since discontinuities are expected to be present in the flow. The conservative formulation is indeed the best formulation for flows containing discontinuities, since jump relations are contained in the flux expressions. The equations written in total derivative form (4)–(7) and (10), are expressed in conservative variables by combination with the continuity equation (1). The system to be solved is therefore

$$\frac{\partial\rho}{\partial t} + \frac{\partial\rho u}{\partial x} = 0, \tag{13}$$

$$\frac{\partial\rho u}{\partial t} + \frac{\partial(\rho u^2 + P)}{\partial x} = 0, \tag{14}$$

$$\frac{\partial\rho E}{\partial t} + \frac{\partial u(\rho e^2 + P)}{\partial x} = 0, \tag{15}$$

$$\frac{\partial\rho\lambda}{\partial t} + \frac{\partial\rho\lambda u}{\partial x} = \mu\left(\frac{\partial\rho f}{\partial t} + \frac{\partial\rho f u}{\partial x}\right) + (1-\mu)\left(\frac{\partial\rho g}{\partial t} + \frac{\partial\rho g u}{\partial x}\right), \tag{16}$$

$$\frac{\partial\rho f}{\partial t} + \frac{\partial\rho f u}{\partial x} = \rho(1-f)Z\frac{\alpha\beta}{\theta^2}\mathrm{e}^{-\alpha/\theta}, \tag{17}$$

$$\frac{\partial\rho g}{\partial t} + \frac{\partial\rho g u}{\partial x} = \begin{cases} 0 & \text{if } f < f_0, \\ (1-g)\dfrac{f-f_0}{1-f_0}[G_0 + F(P_{\text{shock}})]\left(\dfrac{P}{P_0}\right)^r & \text{if } f > f_0, \end{cases} \tag{18}$$

$$\frac{\partial\rho P_{\text{shock}}}{\partial t} + \frac{\partial\rho u P_{\text{shock}}}{\partial x} = 0. \tag{19}$$

This system is accompanied by the closure laws (8), (9) and (11). The system of equations to be solved is obviously hyperbolic. We are now going to suggest a strategy for its solution.

 

## 3. THE METHOD

As mentioned in Section 1, the method presented here is fully Eulerian and uses previous works that have elaborated typical second-order Godunov schemes. Section 4 will be devoted to an extension of this method to a shock-tracking variant. The van Leer concept[2] is distinguished from that of Godunov[1] by the following fundamental idea: flow variables are considered as piecewise linear functions over the computational domain. In the Godunov method these functions are assumed to be piecewise constants. Thus each conservative variable is characterized in each cell by an average value and a slope. The conservative variable vector is denoted by

$$U = (\rho, \rho u, \rho E, \rho\lambda, \rho f, \rho g, \rho P_{\text{shock}})^{\text{T}}.$$

The system composed of equations (13)–(15) constitutes the Euler equations, while system (16)–(19) constitutes the species equations by analogy with the terminology used in reactive flows. The overall system to be solved is hyperbolic and conservative. It can be written in the form

$$\frac{\partial U}{\partial t} + \frac{\partial F(U)}{\partial x} = S(U), \tag{20}$$

where $F(U)$ represents the flux vector in (13)–(19) and $S(U)$ the source terms.

### 3.1. Time splitting

With the present model one expects that source terms, representing chemical decomposition reactions, will depend strongly on the hot spot temperature and shock pressure. It is therefore preferable to solve source terms by an implicit technique or with the help of a good differential solver. Thus, in order to avoid costly matrix operations and to use the best method for the hyperbolic system, a time-splitting procedure is employed in which hydrodynamic and chemical processes evolve independently during a time step. The time-splitting technique follows the ideas of Strang.[15] Thus for equation (20) the solution will be obtained by a succession of operators as

$$U^{n+1} = L_{\text{s}}^{\Delta t/2} L_{\text{f}}^{\Delta t} L_{\text{s}}^{\Delta t/2} U^n. \tag{21}$$

The operator $L_{\text{s}}^{\Delta t/2}$ represents the numerical solution of the ordinary differential system where only source terms are present, i.e.

$$\frac{\partial U}{\partial t} = S(U). \tag{22}$$

This stage is realized with the help of the DVODE solver,[16] which possesses the feature of being able to adapt automatically the time step and the integration method according to the problem stiffness. No additional calculation is needed (Jacobian matrix, for example) for its use.

The operator $L_{\text{f}}^{\Delta t}$ represents the numerical solution of the hyperbolic system

$$\frac{\partial U}{\partial t} + \frac{\partial F(U)}{\partial x} = 0, \tag{23}$$

which constitutes a more difficult stage for its resolution than problem (22). Essentially, two strategies are possible. The first consists of adapting Roe's method[3] to solve the equations. The second alternative resides in the original methodology of van Leer with the MUSCL method. For Roe's method it is necessary to calculate eigenvalues and eigenvectors of Roe's matrix. Such operations are particularly tedious for sufficiently high-dimensional systems (more than three) and compromise rapid modifications of the equation model to be solved. These operations become more complex as the equation of state increases in complexity. Moreover, the development of a linearized

 

Riemann solver by Roe's strategy for real gases, following Glaister,[17] is not easy for the equation of state involving three parameters that we must consider. In summary, we conclude that Roe's method is too costly to implement for classical detonation applications, although its accuracy and qualities are not debatable. For example, one can refer to the excellent paper of Clarke *et al.*[18] to see the capabilities of this method on a detonation problem involving, albeit, a rather simplified model. One returns therefore to the MUSCL strategy that does not require as many operations and that, with the proposed adjustment, will lead to an accuracy comparable with that of Roe's method. This method consists of a succession of several steps:

(a) prediction of conservative variables at instant $n+\frac{1}{2}$ on each cell interface
(b) resolution of the Riemann problem by an exact or approximate solver
(c) application of the conservative law on each control volume
(d) limitation of slope variables on each cell.

### 3.2. Predictor

Stage (a) may be undertaken essentially by following two strategies which have proven their efficiency: the PLM (piecewise linear method) due to Colella and Glaz[19] (see also Reference 4) and the MUSCL–Hancock procedure described by Quirk.[20] The PLM requires calculation of the system Jacobian matrix (23). The operation is possible but is rendered tedious by the complex equation of state that we have to manipulate. We recommend the MUSCL–Hancock procedure because it leads to the same accuracy as the PLM without recourse to the Jacobian matrix calculation. In this context the predictor step is written as follows.

Consider first a control volume $i$ whose interfaces are identified as $i+\frac{1}{2}$ and $i-\frac{1}{2}$ (Figure 1). In cell $i$ the vector $U_i^n$ and the slopes $\delta U_i^n$ of conservative variables are known at the current time $n$.

One first expresses the conservative variables on the cell interfaces at time $n$, viewed from the cell interior:

$$U^n_{i+1/2,\mathrm{L}} = U_i^n + \tfrac{1}{2}\delta U_i^n, \qquad U^n_{i-1/2,\mathrm{R}} = U_i^n - \tfrac{1}{2}\delta U_i^n. \tag{24}$$

Then the evolution of these variables at time $n+\frac{1}{2}$ is determined using the fluxes calculated with the help of the previous variables and the discretization of equation (23):

$$\begin{aligned} U^{n+1/2}_{i+1/2,\mathrm{L}} &= U^n_{i+1/2,\mathrm{L}} - \frac{\Delta t}{2\Delta x}[F(U^n_{i+1/2,\mathrm{L}}) - F(U^n_{i-1/2,\mathrm{R}})], \\ U^{n+1/2}_{i-1/2,\mathrm{R}} &= U^n_{i-1/2,\mathrm{R}} - \frac{\Delta t}{2\Delta x}[F(U^n_{i+1/2,\mathrm{L}}) - F(U^n_{i-1/2,\mathrm{R}})]. \end{aligned} \tag{25}$$

Note that it is not necessary to apply this procedure to the entire set of equations (13)–(19). Indeed, in order for the method to be second-order-accurate, it is necessary that the conservative variables be piecewise linear functions. Concerning equations (16)–(19), the variable $\rho$ being a piecewise linear

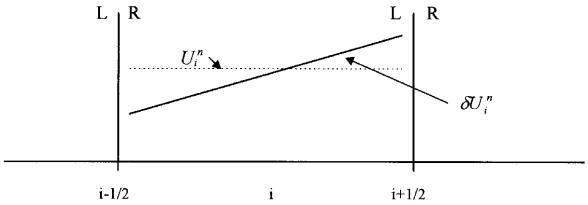


Figure 1. Representation of conservative variable evolution in fixed one-dimensional control volume

 

function, it suffices that the primitive variables ($\lambda, f, g$ and $P_{\text{shock}}$) be piecewise constant functions. In this situation the predictor step for equations (16)–(19) reduces to

$$U^{n+1/2}_{i\pm1/2,\text{LR}} = \frac{\rho^{n+1/2}_{i\pm1/2,\text{LR}}}{\rho^n_i} U^n_i. \tag{26}$$

### 3.3. Riemann problem

Stage (b) is devoted to the Riemann problem solution and constitutes the most difficult part of the present algorithm. As we have already mentioned, Glaister's method is too intricate to implement for present applications, in which the equation of state is a function of more than two variables. It is again necessary to choose between three alternatives: the quasi-exact solver of Saurel *et al.*,[21] the approximate solver of Harten *et al.*[22] (HLL) and the flux-splitting technique of van Leer extended to real gases by Liou *et al.*[23] Riemann solvers based on flux splitting have shown some weaknesses in the resolution of several problems in gas dynamics with the ideal gas equation of state. One therefore excludes this possibility. The Riemann solver of Saurel *et al.*[21] is very accurate but is also the most complicated of the three. It requires in the case of a two-variable equation of state a significant number of thermodynamic function calculations. Although this is possible, it is difficult to generalize the technique to an equation of state that is a function of three variables. Therefore it is not adopted for the present problem. Thus only the HLL approximate solver[22] remains. It requires as input all right- and left-state fluid variables and also wave speed estimates for the right- and left-facing waves. Knowledge of these wave speeds is not *a priori* evident. Usually, these wave speeds are outputs of Riemann solver. The HLL solver therefore requires part of the solution. These wave speed estimates may be determined with satisfactory accuracy by the Davis approximation.[24] Another disadvantage of this solver is that it provides only an average state for density and internal energy between the right- and left-facing waves (Figure 2). The presence of the contact surface between the right- and left-facing waves implied a density and internal energy discontinuity across right- and left-facing waves. It would therefore be prejudicial to have a unique average state between the two waves. This disadvantage has been remedied by Toro *et al.*,[25] whereby the contact surface is restored in the HLL solver. With this correction it is called the HLLC solver. We recall briefly the basic ideas of this clever Riemann solver. Equation (23) is written in integral form (27), in order to admit discontinuous solutions, as

$$\int_\Omega [U\,\mathrm{d}x - F(U)\,\mathrm{d}t] = 0. \tag{27}$$

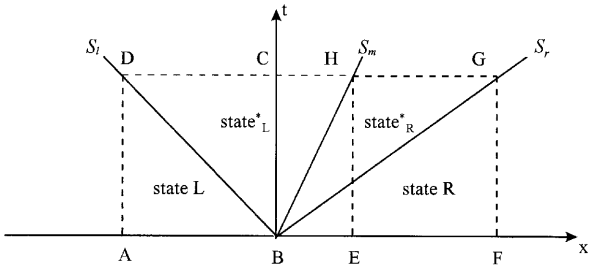


Figure 2. Representation of Riemann problem between states $U_\text{L}$ and $U_\text{R}$ according to HLLC approximation

 

For a control volume of dimensions $[x_1, x_2] \times [t_1, t_2]$, equation (27) becomes

$$\int_{x_1}^{x_2} U(x, t_2)\, \mathrm{d}x - \int_{x_1}^{x_2} U(x, t_1)\, \mathrm{d}x + \int_{t_1}^{t_2} F(U(x_2, t))\, \mathrm{d}t - \int_{t_1}^{t_2} F(U(x_1, t))\, \mathrm{d}t = 0. \tag{28}$$

Following Toro,[7] integration (28) is performed over the control volumes schematized in Figure 2. $U_{\mathrm{L}}^*$ and $U_{\mathrm{R}}^*$ represent the states covered by the left- and right-facing waves respectively and are therefore solutions of the Riemann problem. Note that these states are constant in the approximation of this solver between two waves. Right, left and intermediate wave speeds are denoted by $S_{\mathrm{r}}$, $S_{\mathrm{l}}$ and $S_{\mathrm{m}}$ respectively.

*3.3.1. Wave speed estimates.* The literature provides two possible estimates for the right- and left-facing wave speeds. Davis[24] has proposed as estimate for the right-facing wave speed the maximum speed of characteristic waves, i.e. $S_{\mathrm{R}} = \max(u_{\mathrm{l}} + c_{\mathrm{l}}, u_{\mathrm{r}} + c_{\mathrm{r}})$. By the same reasoning the left-facing wave speed is obtained as $S_{\mathrm{L}} = \min(u_{\mathrm{l}} - c_{\mathrm{l}}, u_{\mathrm{r}} - c_{\mathrm{r}})$. Note that this estimate uses only known variables from right and left states. Another possible choice is that proposed by Einfeld *et al.*[26] This estimate uses Roe-averaged variables. As already mentioned, we consider the calculation of these variables too complex and costly for the non-ideal equations of state employed here. We therefore retain the wave speed estimates of Davis.[24] This choice may be improved using relation (31) following recommendations by Toro *et al.*[25] It remains now to determine the contact surface velocity $S_{\mathrm{m}}$. Evaluation of the integral (28) over the control volume ABCD yields

$$U_{\mathrm{L}}^* = U_{\mathrm{L}} + \frac{F_{\mathrm{L}}^* - F_{\mathrm{L}}}{S_{\mathrm{L}}}. \tag{29}$$

Similarly, integration over the control volume BFGC gives

$$U_{\mathrm{L}}^* = U_{\mathrm{R}} + \frac{F_{\mathrm{L}}^* - F_{\mathrm{R}}}{S_{\mathrm{R}}}. \tag{30}$$

Combination of relationships (29) and (30) yields the result

$$U_{\mathrm{L}}^* = \frac{S_{\mathrm{R}} U_{\mathrm{R}} - S_{\mathrm{L}} U_{\mathrm{L}} - (F_{\mathrm{R}} - F_{\mathrm{L}})}{S_{\mathrm{R}} - S_{\mathrm{L}}}. \tag{31}$$

One can notice that this result is indifferent to whether the contact surface faces right or left. Equation (31) represents the Riemann problem solution in the original framework of the HLL solver. Here equation (31) allows the calculation of the speed $S_{\mathrm{m}}$ by taking the ratio of the first two conservative variables. Also, the $S_{\mathrm{R}}$ and $S_{\mathrm{L}}$ estimates may be improved with the help of the $U_{\mathrm{L}}^*$ state. See Reference 25 for recommendations.

*3.3.2. Complete solution.* Equation (29) can be written in the form

$$S_{\mathrm{L}} U_{\mathrm{L}}^* - F_{\mathrm{L}}^* = S_{\mathrm{L}} U_{\mathrm{L}} - F_{\mathrm{L}}. \tag{32}$$

Note that the right-hand side of this equation is known. The mass flux for the fluid crossed by the left-facing wave is written as $F_{\mathrm{L}}^* = \rho_{\mathrm{L}}^* u_{\mathrm{L}}^*$. This equation makes intervene the fluid velocity between the right- and left-facing waves, determined previously. Indeed, $u_{\mathrm{L}}^* = u_{\mathrm{R}}^* = S_{\mathrm{m}}$. One then determines

$$\rho_{\mathrm{L}}^* = \rho_{\mathrm{L}} \frac{S_{\mathrm{L}} - u_{\mathrm{L}}}{S_{\mathrm{L}} - S_{\mathrm{m}}}. \tag{33}$$

 

By the same reasoning the other variables to the left of the contact surface are obtained. The variables to the right of the contact surface are obtained by performing the integral (28) over the control volume EFGH to give

$$F_{\mathrm{R}}^{*} = F_{\mathrm{R}} + S_{\mathrm{R}}(U_{\mathrm{R}}^{*} - U_{\mathrm{R}}), \tag{34}$$

yielding the density expression

$$\rho_{\mathrm{R}}^{*} = \rho_{\mathrm{R}} \frac{S_{\mathrm{R}} - u_{\mathrm{R}}}{S_{\mathrm{R}} - S_{\mathrm{m}}}. \tag{35}$$

*Remark.* As for the predictor step, it is not necessary to perform all these calculations for the complete system (23). Resolution of the Riemann problem is indispensable for the Euler equations (13)–(15) but is not necessary for the species equations (16)–(19). Writing these equations in primitive variables shows that the variables $\lambda, f, g$ and $P_{\mathrm{shock}}$ are constant along the characteristic direction $\mathrm{d}x/\mathrm{d}t = u$. It follows that these variables undergo no variation across the right- and left-facing waves. Determination of the contact surface velocity is therefore sufficient to know the upwinding sense for the various flux calculations.

### 3.4. Conservation step

This step proceeds without difficulty. The solution is obtained by integrating equation (23) over the control volume:

$$U_i^{n+1} = U_i^n - \frac{\Delta t}{\Delta x}[F(W_{\mathrm{R}}) - F(W_{\mathrm{L}})]. \tag{36}$$

States $W_{\mathrm{R}}$ and $W_{\mathrm{L}}$ represent the Riemann problem solution detailed previously from states calculated during the predictor step:

$$W_{\mathrm{R}} = W_{\mathrm{R}}\left(U_{i+1/2,\mathrm{L}}^{n+1/2}, U_{i+1/2,\mathrm{R}}^{n+1/2}\right), \qquad W_{\mathrm{L}} = W_{\mathrm{L}}\left(U_{i-1/2,\mathrm{L}}^{n+1/2}, U_{i-1/2,\mathrm{R}}^{n+1/2}\right). \tag{37}$$

Sampling of the Riemann problem solution state depends on the relative intercell line position $(x/t = 0)$ and on the various right, left and intermediate wave speeds.

### 3.5. Limitation process

There exist various procedures for slope limitation in order to obtain monotonicity. Three flux limiters have been tested: the Minmod,[2] Van Albada *et al.*[27] and Superbee[28] limiters. The Superbee limiter[28] is reputed for its excellent resolution of discontinuities. However, it produces prejudicial oscillations. The Minmod limiter[2] is more diffusive for discontinuities but produces no parasitic oscillations. The Van Albada *et al.* limiter[27] lies between the two previous limiters for the capture of discontinuities and does not create parasitic oscillations. Denoting $\delta U_i^{+} = U_{i+1} - U_i$, $\delta U_i^{-} = U_i - U_{i-1}$, $\Sigma = \delta^{+} + \delta^{-}$ and $\pi = \delta^{+}\delta^{-}$,

$$\text{if } \Sigma > \varepsilon, \text{ then } \delta U_i = \frac{\pi + |\pi|}{\Sigma}, \text{ else } \delta U_i = 0 \quad (\varepsilon = 10^{-12} \text{ in our calculations}). \tag{38}$$

The slope calculations proposed here make use of conservative variables. Other choices are possible, namely characteristic or primitive variables. Slope calculations in the primitive variable formulation yield a degradation of the solution in comparison with the conservative formulation. The characteristic variable formulation has been tested by the authors on an ideal gas test case. It

 

improves the solution in comparison with conservative slopes but does not guarantee robustness of the scheme when subjected to the drastic conditions that we are treating.

### 3.6. Numerical tests

Figures 3–6 present a comparison between the various schemes mentioned in Section 1 and the new algorithm given here. The test case is the classical shock tube problem. For this test case the ideal gas equation of state has been employed in order to compare computed results with the available exact solution. Only density profiles are represented. Conditions of the test problem are: left state—$P = 0{\cdot}1$ GPa, $\rho = 10\,\mathrm{kg\,m^{-3}}$, $u = 0\,\mathrm{m\,s^{-1}}$; right state—$P = 0{\cdot}1$ MPa, $\rho = 1\,\mathrm{kg\,m^{-3}}$, $u = 0\,\mathrm{m\,s^{-1}}$. The tube is filled in its right and left chambers by the same gas of specific heat ratio $\gamma = 1{\cdot}4$. Initially, the separation between the left and right chambers is located at the middle of the shock tube. Results are reported at time $80\,\mu$s. A constant time step of $1\,\mu$s has been used in all calculations. The exact solution is always shown as a full curve, while the numerical solution is shown as a series of points. In all cases the mesh contains 100 cells.

Figure 3 shows results obtained for this test case with the MacCormack[10] scheme. A second-order artificial viscosity correction is used following MacCormack. The artificial viscosity coefficient has been chosen equal to 0·03 and corresponds to the best compromise for wave capturing in this test case. This scheme is very representative of the class of methods currently used in detonation codes. One can notice that the shock wave capture is within four grid points and that the contact discontinuity is within 10 grid points approximately. Oscillations are present for each discontinuity. The rarefaction wave, on the other hand, is computed correctly.

Figure 4 shows the results obtained with the Godunov[1] scheme. The performance of this scheme in terms of discontinuity handling is comparable with that of the MacCormack scheme. However, the density plateau is not reached and the rarefaction wave is less resolved. Nevertheless, no oscillation is present.

In Figure 5 the second-order Godunov scheme described previously has been used. The Riemann solver is HLLC and the flux limiter is Superbee. The shock wave and the contact discontinuity are now captured within two and six grid points respectively. The rarefaction wave is solved perfectly. On the other hand, the tail of the rarefaction wave (abscissa 0·6 m) produces a strong oscillation. Note that the density plateau is nearly reached.

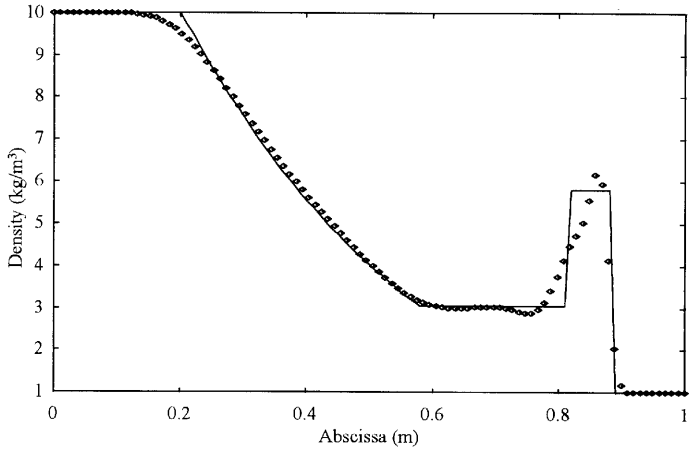


Figure 3. Density profile for shock tube case test with MacCormack scheme

 

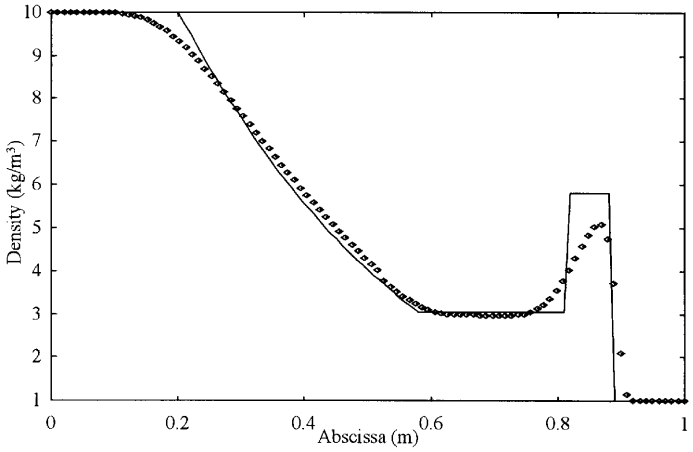


Figure 4. Density profile for shock tube test case with Godunov scheme

Results of Figure 6 are similar to those of Figure 5. The oscillation at the tail of the rarefaction wave has nearly disappeared, but the contact discontinuity is more diffused. The preceding test case puts in evidence the superiority of second-order Godunov-type schemes, even if they are perfectible. The Van Albada *et al.* limiter seems to be a good compromise.

Before applying the proposed scheme to a detonation problem, it is necessary to clarify an aspect not emphasized yet. The chemical decomposition model of the explosive which is employed here is that of Johnson *et al.*[11] as described in Section 2. It uses the shock pressure as parameter. However, it is well known that Eulerian methods do not allow the determination of the shock pressure, since shock waves are always diffused over several meshes. Two ways are nevertheless possible to determine the shock pressure: (i) the use of a sensor which detects the shock wave passage; (ii) the development of a shock-tracking algorithm which eliminates shock wave diffusion.

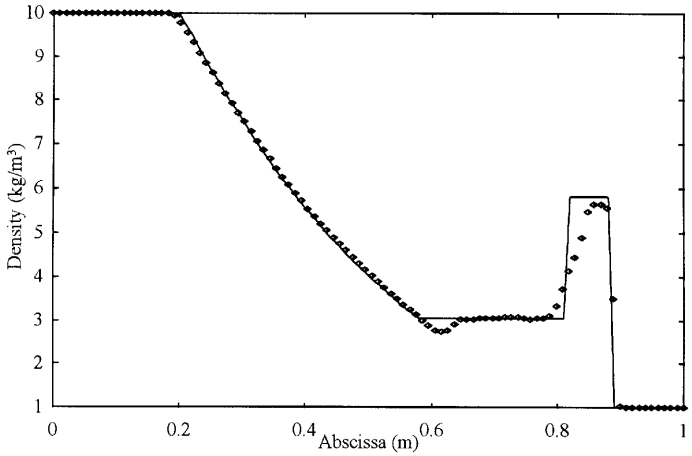


Figure 5. Density profile for shock tube test case with present scheme and Superbee limiter

 

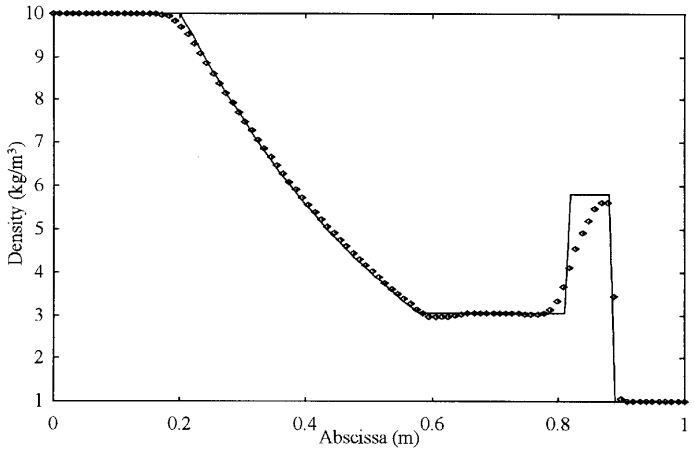


Figure 6. Density profile for shock test tube test case with present scheme and Van Albada *et al.* limiter

The second alternative is more complicated to implement than the first. Nevertheless, we are going to develop this approach in the sequel. For the moment we use as shock wave sensor the following criterion:

$$\text{if } \Delta = u_{i+1} - u_{i-1} < 0, \text{ then } S_{\text{shock}} = \frac{\rho}{P}\Delta^2, \text{ otherwise } S_{\text{shock}} = 0. \tag{39}$$

The shock wave is considered to have crossed a cell if the following criteria are satisfied: $P_i > P_{\text{shock}}$ and $S_{\text{shock},i} < 0{\cdot}01$ (for example). $P_{\text{shock}}$ is a threshold pressure, taken as equal to half the impact pressure for the present application. The test case studied is that of a shock-to-detonation transition of a high explosive, PBX 9404, whose data are listed in Table I.

An impactor, made of the same material as the explosive, hits a 2 cm long column of the explosive. The impactor has a velocity of $530\,\text{m s}^{-1}$ and induces a 3·5 GPa shock wave in the explosive. The induced shock wave provokes the initiation of a combustion that gradually grows to a detonation. During the whole calculation the inlet boundary condition is treated as a moving piston with a velocity of $530\,\text{m s}^{-1}$.

The pressure evolution in the column at equally spaced time instants (0·3 ms) has been plotted during the shock-to-detonation transition process. In the first curve (Figure 7) the shock wave has just penetrated the explosive and the reaction is not significant enough to cause any variation in the pressure. In the second curve the reaction has begun. The pressure is slightly higher and the shock wave a little more intense. This effect is emphasized in the next three curves. In the fifth curve it appears clearly that the combustion has hold of the shock wave. In the next curve, catching up has occurred and the pressure curve becomes very stiff. Detonation has been achieved. The subsequent curves show the stabilization of this detonation.

Figure 8 shows the pressure signal recorded by equally spaced fluid volumes, initially of 1 mm, over a distance of 10 mm. These volumes are free to displace in a Lagrangian manner. The previously mentioned phenomena are better visible. The detonation appears at a Lagrangian abscissa of 7 mm.

Figure 9 shows the evolution of the shock wave sensor at the same instants as in Figure 7. This sensor allows the calculation of the shock pressure as presented in Figure 10.

To check the validity of the shock pressure determination process, we are now going to develop a shock-tracking variant of the proposed method.

 

Table I. Physical data for PBX 9404 (MKS units)

| CC EOS | Parameter | JWL EOS | Parameter |
|---|---|---|---|
| $A_1$ | $1{\cdot}287 \times 10^{10}$ | $A$ | $8{\cdot}545 \times 10^{11}$ |
| $A_2$ | $1{\cdot}342 \times 10^{10}$ | $B$ | $2{\cdot}050 \times 10^{10}$ |
| $E_1$ | 4·1 | $R_1$ | 4·6 |
| $E_2$ | 3·1 | $R_2$ | 1·35 |
| $C_{vs}$ | 1087 | $C_{vg}$ | 815 |
| $\Gamma_{s0}$ | 0·93 | $\Gamma_{g0}$ | 0·25 |
| **JTF kinetics** | **Parameter** | **General** | **Parameter** |
| $P_0$ | $3{\cdot}5 \times 10^9$ | ID[a] | 1840 |
| $\mu$ | 0·05 | $D_{CJ}$ | 8800 |
| $\theta_0$ | 725 | $P_{CJ}$ | $37 \times 10^9$ |
| $m$ | 3 | $T_{CJ}$ | 4040 |
| $\Gamma_k$ | $4 \times 10^{-12}$ | | |
| $Z$ | $5 \times 10^{19}$ | | |
| $\alpha$ | 26520 | | |
| $\beta$ | 2500 | | |
| $f_0$ | 0·14 | | |
| $G_0$ | $1{\cdot}015 \times 10^6$ | | |
| $A$ | 116987 | | |
| $B$ | 0 | | |
| $n$ | 2·811 | | |
| $r$ | 1 | | |

[a] Initial density.

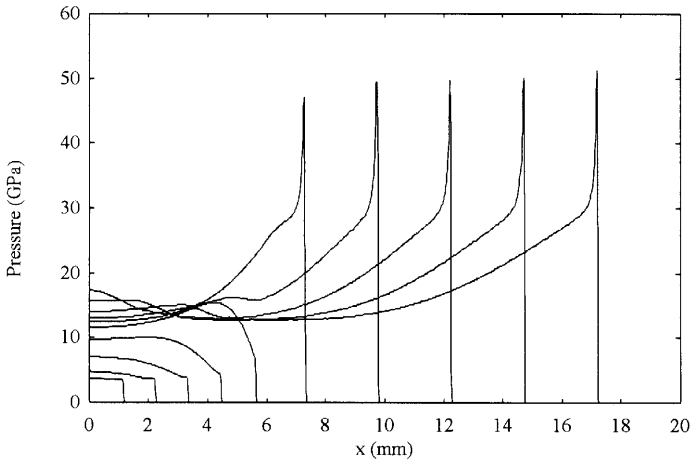


Figure 7. Pressure evolution in column of explosive

## 4. THE SHOCK-TRACKING VARIANT

The shock-tracking method requires more thought to implement than the previous Eulerian scheme. In the one-dimensional case the modifications are not very complex and the implementation is quite accessible. The two-dimensional extension is more difficult because it is necessary to track a 2D curve. The necessary elements for the implementation of a two-dimensional front-tracking method

 

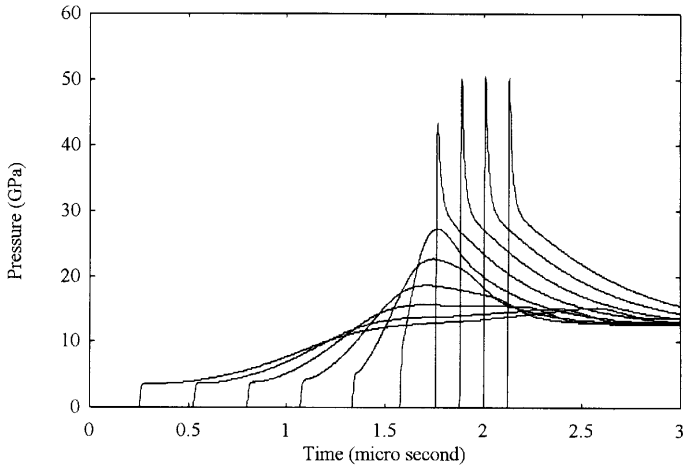


Figure 8. Pressure evolution on Lagrangian scale

can be found in References 29 and 30. The latter paper details how to follow a two-dimensional interface. The basic ideas can be extended to shock tracking.

We consider here only one-dimensional shock tracking. The necessity of this type of algorithm has been especially emphasized by Bukiet,[31] who has developed an extension of the random choice method of Glimm[32] to solid explosive detonations. The solution of the Riemann problem in reactive flow has been detailed, but the equation of state used is very simplified, since the ideal gas law is used. Here the model described in Section 2 is used, with the equations of state and complex kinetics mentioned previously.

The shock position is known initially and its current position is determined by solution of the equation

$$\frac{\mathrm{d}X_\mathrm{s}}{\mathrm{d}t} = \omega_\mathrm{s}. \tag{40}$$

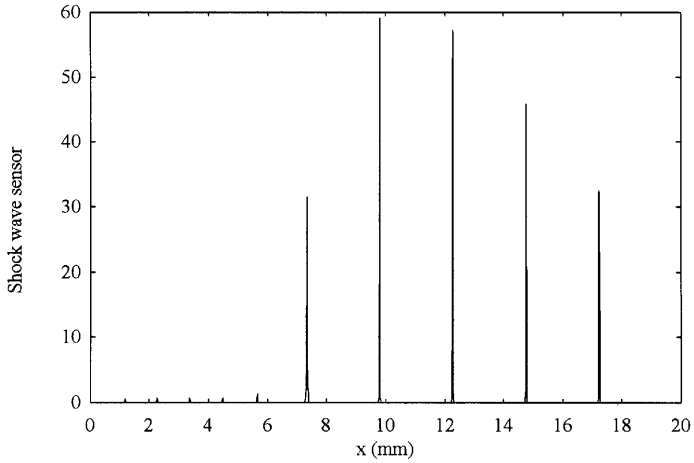


Figure 9. Evolution of shock wave sensor

 

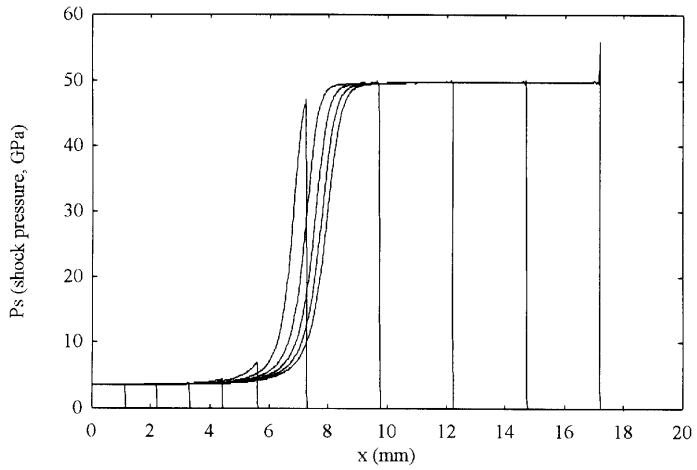


Figure 10. Evolution of shock pressure

The current position of the shock wave allows the determination of the cell index where the shock is situated ($I_s$). Two configurations are then possible according to whether the shock remains in the cell $I_s$ between two successive instants or leaves it.

(a) *The shock remains in the cell.* This situation is represented in Figure 11, where the broken lines represent interfaces between two cells. Up to point $I_s - 1$ these interfaces are motionless and so the Eulerian method described previously can be used. For cell $I_s$ the interface $I_s - \frac{1}{2}$ is motionless, but the interface on the right, represented by the shock, displaces with velocity $\omega_s$. Thus the control volume varies with time. The conservation law then becomes

$$U_i^{n+1} = \frac{1}{\Delta x^{n+1}}\left(\Delta x^n U_i^n + \frac{\Delta t}{\Delta x^n}[F(W_R) - F(W_L)]\right),$$
$$\Delta x^n = X_s^n - x_{I_s-1/2}, \qquad \Delta x^{n+1} = X_s^{n+1} - x_{I_s-1/2} \tag{41}$$

and $W_R$ and $W_L$ represents the Riemann problem solution calculated from the states

$$W_L = W_L(U_{I_s-1}^n, U_{I_s}^n), \qquad W_R = W_R(U_{I_s+1}^n, U_{I_s+1}^n). \tag{42}$$

In order to solve the Riemann problem between states $U_{I_s}^n$ and $U_{I_s+1}^n$, the right wave speed $S_R = \omega_s$ (shock wave speed) is necessary for the HLLC solver. $\omega_s$ is determined by resolution of the Rankine–

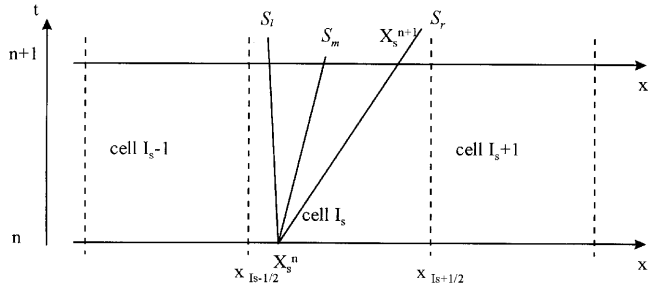


Figure 11. Shock remaining inside cell

 

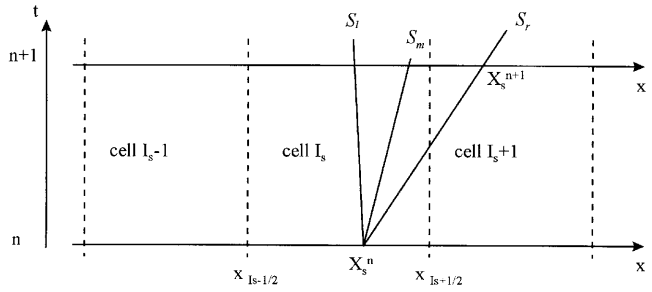


Figure 12. Shock changing cell

Hugoniot conditions between states $U_{I_s}^n$ and $U_{I_{s+1}}^n$. Finally, it is necessary to take the shock motion into account for the flux calculation at the moving boundary corresponding to the shock wave:

$$F(W_R) = \begin{cases} \rho(u-\omega_s) \\ \rho(u-\omega_s)u + P \\ \rho(u-\omega_s)E + Pu \end{cases}$$

(b) *The shock leaves the cell.* This situation is represented in Figure 12. In this case, cells 1 to $I_s - 1$ and cells $I_s + 2$ to $I_{end}$ (if necessary) are processed by the Eulerian algorithm. The cell $I_s$ is processed by the preceding procedure. The cell $I_s + 1$ is allocated directly by the state solution of the Riemann problem:

$$\text{if } X_s^{n+1} > x_{I_s+1} \text{ and } X_{\text{contact}}^{n+1} < x_{I_s+1}, \text{ then } U_{I_s^{n+1}} = U_R^*;$$
$$\text{if } X_s^{n+1} > x_{I_s+1} \text{ and } X_{\text{contact}}^{n+1} > x_{I_s+1}, \text{ then } U_{I_s^{n+1}} = U_L^*;$$

We use the same shock-to-detonation transition test case as previously. Results shown in Figure 13 are to be compared with those in Figure 7. One can notice that the problem of shock-to-detonation transition is solved as well by the Eulerian method as by the shock-tracking method. Shock fronts are

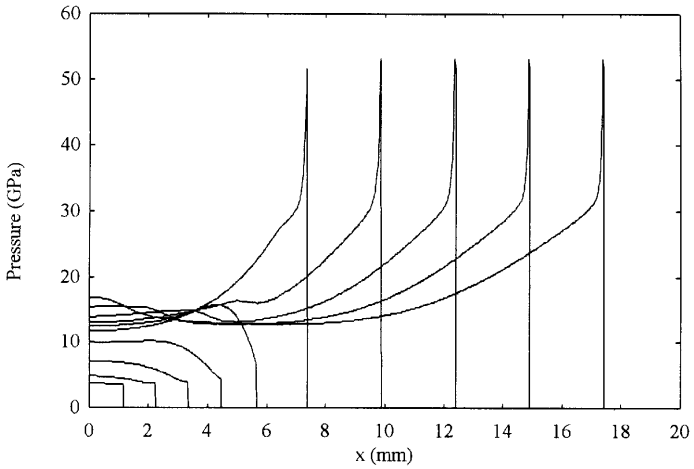


Figure 13. Pressure evolution in column of explosive

 

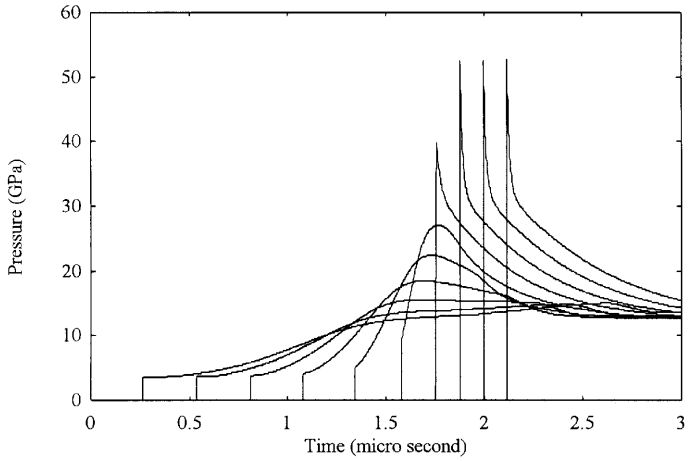


Figure 14. Pressure evolution on Lagrangian scale

more sharply resolved. Differences between the two methods are not readily visible, because a fine mesh has been used involving 1000 uniformly distributed cells.

The benefit of shock wave capturing is more clearly seen in Figure 14 by comparison with Figure 8. The detonation is identically observed at the Lagrangian abscissa of 7 mm, but the pressure rise at the Neumann spike reaches a slightly inferior level compared with the full Eulerian calculation. In Figure 15 the shock pressure evolution is presented and can be compared with the evolution of Figure 10. The new results are very close, which allows one to validate the calculation of the shock pressure in the context of the Eulerian method. One can also notice that the shock-tracking method eliminates all parasitic oscillations in the simulation. In order to validate results produced by the two codes. Eulerian and shock tracking, another code has been realized to solve the flow in the detonation reaction zone. This type of calculation can be achieved by following the basic ideas of the ZND model resolution as presented by Fickett and Davis.[33] Recall only that this model is valid in the context of a steady plane detonation. By writing the one-dimensional hydrodynamics equations in the steady regime and in the shock wave frame of reference, one can calculate the shock flow variables

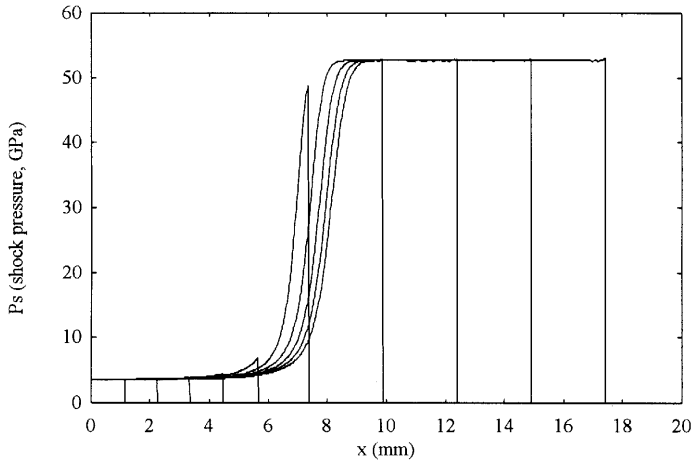


Figure 15. Evolution of shock pressure

 

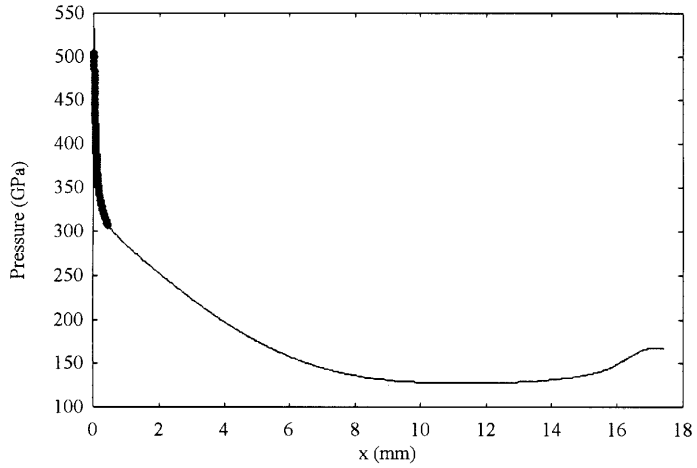


Figure 16. Pressure evolution for stable detonation, calculated with ZND model (bold curve) and shock-tracking method (full curve)

up to the sonic point (CJ point). This calculation involves the solution of a simple ordinary differential system that is easy to solve and does not involve wave dynamics. These results can therefore serve as validation for the shock-tracking code.

In Figure 16 the evolution of the pressure is presented, starting from the shock front back to flow. The full curve relates to the shock-tracking calculation. The bold curve, appearing only in the reaction zone, relates to the ZND model resolution. The agreement between the two simulations is good, thus validating the tracking code and the Eulerian approach.

## 5. CONCLUSIONS

Two efficient approaches for the solution of detonation dynamics in a high explosive have been presented. A full Eulerian approach based on a TVD scheme, adapted to real gases with a complex equation of state, has been developed. An extention of this method to shock tracking has been proposed. These two methods are based on the Riemann problem, which has been solved approximately using the Toro *et al.*[25] Riemann solver. The two methods are efficient, robust and accurate. The Eulerian tracking method has the advantage of being easily extensible to multidimensional problems. The shock-tracking method is generalizable in 2D but difficult to conceive in 3D. We therefore propose to use this type of approach for one-dimensional problems essentially. This approach can replace the usual resolution methodology of the ZND problem. It allows the calculation of the flow variables in the reaction zone and outside. It can be used for detonation wave acceleration that cannot be calculated by the usual ZND methods. The shock-tracking version is faster than the Eulerian method, since the calculation is restricted to the cells from the inlet of the tube up to the shock. As it is more accurate than the Eulerian version, since it does not suffer from numerical diffusion at the shock wave, it may be used for the determination of the optimal mesh size for the Eulerian code. Indeed, on the test case presented, results between the two versions are identical using 200 cells. Results are again very close using 100 cells. One can therefore use the tracking version as reference to determine in one dimension the optimal mesh for the Eulerian version. For multidimensional problems the Eulerian version is recommended because of its compromise between accuracy and simplicity.

 

ACKNOWLEDGEMENTS

This study has been supported by DGA/DRET/ETCA/CEG. We particularly thank Mr. J. C. Goutelle for having proposed this subject to us. We also acknowledge Professor P. B. Butler for his help in editing of this paper.

## APPENDIX: EQUATIONS OF STATE

The Cochran–Chan[14] equation of state (EOS) is a complete equation of state that is normally used to describe solid material behaviour under shock waves. This EOS can be written in Mie–Gruneisen form as

$$P(\rho, e) = \rho\Gamma_{s0}[e - e_{ks}(\rho)] + P_{ks}(\rho),$$

where

$$e_{ks}(\rho) = -\frac{A_1}{\rho_0(1-E_1)}\left[\left(\frac{\rho_0}{\rho}\right)^{1-E_1} - 1\right] + \frac{A_2}{\rho_0(1-E_2)}\left[\left(\frac{\rho_0}{\rho}\right)^{1-E_2} - 1\right] - C_{vs}T_0 + e_0,$$

$$e(\rho, T) = e_{ks}(\rho) + C_{vs}T,$$

The squared sound speed is given by

$$c^2 = \frac{1}{\rho}(\Gamma_{s0} + 1)(P - P_{ks}) + \frac{\mathrm{d}P_{ks}}{\mathrm{d}\rho}.$$

The Jones–Wilkins–Lee (JWL) EOS is normally used for gaseous detonation products and can be written in Mie–Gruneisen form, following Baudin and Bergues,[12] as

$$P(\rho, e) = \rho\Gamma_{g0}[e - e_{kg}(\rho)] + P_{kg}(\rho),$$

where

$$e_{kg}(\rho) = \underbrace{\frac{A}{\rho_0 R_1}\mathrm{e}^{-R_1(\rho_0/\rho)} + \frac{B}{\rho_0 R_2}\mathrm{e}^{-R_2(\rho_0/\rho)} + c_{e_k}T_0}_{e_{k1}} + \underbrace{\frac{k}{\rho_0\Gamma_{g0}}\left(\frac{\rho_0}{\rho}\right)^{-\Gamma_0}}_{e_{k2}},$$

$$E(\rho, T) = e_{kg}(\rho) + C_{vg}T,$$

$$P_{kg}(v) = -\frac{\mathrm{d}e_{kg}}{\mathrm{d}(1/\rho)} = \underbrace{A\mathrm{e}^{-R_1(\rho_0/\rho)} + B\mathrm{e}^{R_2(\rho_0/\rho)}}_{P_{K1}} + \underbrace{k\left(\frac{\rho_0}{\rho}\right)^{-(\Gamma_{g0}+1)}}_{P_{k2}},$$

$$P(\rho, T) = P_{kg}(\rho) + \rho\Gamma_{g0}C_{vg}T.$$

The constants are given by

$$k = [P_{CJ} - P_{k1}(\rho_{CJ}) - \rho_{CJ}\Gamma_0 C_v T_{CJ}]\left(\frac{\rho_0}{\rho_{CJ}}\right)^{\Gamma_{g0}+1},$$

$$c_{e_k} = -\frac{A}{\rho_0 R_1}\mathrm{e}^{-R_1(\rho_0/\rho CJ)} - \frac{B}{\rho_0 R_2}\mathrm{e}^{-R_2(\rho_0/\rho_{CJ})} - [P_{CJ} - P_{R_1}(P_{CJ})]\frac{1}{\rho_{CJ}\Gamma_{g0}} + e_{CJ},$$

$$\frac{1}{\rho_{CJ}} = \frac{1}{\rho_0} - P_{CJ}\left(\frac{1}{\rho_0 D_{CJ}}\right)^2, \qquad e_{CJ} = \frac{1}{2}P_{CJ}\left(\frac{1}{\rho_0} - \frac{1}{\rho_{CJ}}\right) + e_0.$$

 

The squared sound speed is given by

$$c^2 - \frac{1}{\rho}(\Gamma_{g0} + 1)(P - P_{kg}) + \frac{dP_{kg}}{d\rho}.$$

The CJ parameters can be determined by a CJ thermochemical code (QUERCY,[34] for example). The JWL equation of state corresponds to a reduction of a more complete EOS such as H9.[35] Its coefficients are determined in order to obtain the same CJ point as given by the H9 EOS and the same main isentrope.

A mixture EOS can be constructed as described by Baudin and Bergues,[12] depending on $(\rho, e, \lambda)$ mixture variables:

$$P(\rho, e, \lambda) = \rho\Gamma(\lambda)[e - e_k(\rho, \lambda)] + P_k(\rho, \lambda).$$

The mixture variables are defined by

$$P_k(\rho, \lambda) = (1 - \lambda)P_{ks}(\rho) + \lambda P_{kg}(\rho), \qquad e_k(\rho, \lambda) = (1 - \lambda)e_{ks}(\rho) + \lambda e_{kg}(\rho),$$

$$C_v(\lambda) - (1 - \lambda)C_{vs} + \lambda C_{vg}, \qquad \Gamma(\lambda) = \frac{(1 - \lambda)\Gamma_s C_{vs} + \lambda\Gamma_g C_{vg}}{C_v(\lambda)}.$$

The mixture squared sound speed is given by

$$c^2 = \frac{P - \rho^2(\partial e/\partial\rho)_{P,\lambda}}{\rho^2(\partial e/\partial P)_{\rho,\lambda}}$$

where

$$\left(\frac{\partial e}{\partial\rho}\right)_{P,\lambda} = \left(\frac{\partial e_k}{\partial\rho}\right)_{\lambda} - \left(\frac{(\partial P_k/\partial\rho)_{\lambda}}{\rho\Gamma(\lambda)} + \frac{P - P_k}{\partial^2\Gamma(\lambda)}\right).$$

with $\mu = \rho_0/\rho$ and $d\mu/d\rho = -\rho_0/\rho^2$ one can write

$$\left(\frac{\partial e_k}{\partial\rho}\right)_{\lambda} = \left((1 - \lambda)\frac{de_{ks}}{d\mu} + \lambda\frac{de_{kg}}{d\mu}\right)\frac{d\mu}{d\rho}, \qquad \left(\frac{\partial P_k}{\partial\rho}\right)_{\lambda} = \left((1 - \lambda)\frac{dP_{ks}}{d\mu} + \lambda\frac{dP_{kg}}{d\mu}\right)\frac{d\mu}{d\rho},$$

where

$$\frac{de_{ks}}{d\mu} = -\frac{A_1}{\rho_0}\mu^{-E_1} + \frac{A_2}{\rho_0}\mu^{-E_2}, \qquad \frac{de_{kg}}{d\mu} = -\frac{A}{\rho_0}e^{-R_1\mu} - \frac{B}{\rho_0}e^{-R_2\mu},$$

$$\frac{dP_{ks}}{d\mu} = -A_1E_1\mu^{-(1+E_1)} + A_2E_2\mu^{-(1+E_2)}, \qquad \frac{dP_{kg}}{d\mu} = -AR_1e^{-R_1\mu} - BR_2e^{-R_2\mu},$$

$$\left(\frac{\partial e}{\partial P}\right)_{\rho,\lambda} = \frac{1}{\rho\Gamma(\lambda)}.$$

## REFERENCES

1. S. K. Goduvov, 'A finite difference method for the numerical computation of discontinuous solutions of the equations of fluid dynamics', *Math. Sb.*, **47**, 357–393 (1959).
2. B. van Leer, 'Towards the ultimate conservative difference scheme V. A. second order sequel to Godunov's method', *J. Comput. Phys.*, **32**, 101 (1979).
3. P. L. Roe, 'Approximate Riemann solvers, parameter vectors and difference schemes', *J. Comput. Phys.*, **43**, 357–372 (1981).

 

4. R. Saurel A. Forestier, D. Veyret and J. C. Loraud, 'A finite volume scheme for two-phase compressible flows', *Int. j. numer. meth. fluids*, **18**, 803–819 (1994).
5. R. Saurel, E. Daniel and J. C. Loraud, 'Two phase flows: second order schemes and boundary conditions', *AIAA J.*, **32**, 1214–1221 (1994).
6. R. Saurel 'Numerical analysis of a ram accelerator employing two-phase combustion', *AIAA J. Propuls. Power*, in press.
7. E. F. Toro, *Riemann Solvers and Upwind Methods for Fluid Dynamics*, Springer, Berlin, 1997.
8. P. D. Lax and P. Wendroff, 'Systems of conservation laws', *Commun. Pure Appl. Math.*, 217–237 (1960).
9. R. D. Richtmeyer and K. W. Morton, *Difference Methods for Initial Value Problems*, Interscience–Wiley, New York, 1967.
10. R. W. MacCormack, 'The effect of viscosity in hypervelocity impact cratering', *AIAA Paper 69-354*, 1969.
11. J. N. Johnson, P. K. Tang and C. A. Forest, 'Shock wave initiation of heterogeneous reactive solids', *J. Appl. Phys.*, **57**, (1985).
12. G. Baudin and D. Bergues, 'A reaction model for aluminized PBX applied to underwater explosion calculations', *10th Synmp. on Detonation*, Boston, MA, 1993.
13. E. L. Lee, H. C. Horning and J. W. Kury, 'Adiabatic expansion of high explosives detonation products', *TID 4500-UCRL 50422*, Lawrence Radiation Laboratory, University of California, Livermore, CA, 1968.
14. G. Cochran and J. Chan, 'Shock initiation and detonation models in one and two dimensions', Lawrence Livermore National Laboratory, 1979.
15. G. Strang, 'On the construction and comparison of difference schemes', *SIAM J. Numer. Anal.*, **5**, 506–516 (1968).
16. G. D. Byrne and A. M. Dean, 'The solution of co-polymerization problem with DVODE', in G. D. Byrne and Scheisser (eds), *Results Developments in Numerical Method for ODEs/DAEs/PDEs*, World Scientific, River Edge, NJ, 1992, pp. 137–197.
17. P. Glaister, 'An approximate linearised Riemann solver for the Euler equations for real gases', *J. Comput. Phys.*, **74**, 382–408 (1988).
18. J. F. Clarke, S. Karni, J. J. Quirk, P. L. Roe, L. G. Simmonds and E. F. Toro, 'Numerical computations of two-dimensional unsteady detonation waves in high energy solids', *J. Comput. Phys.*, **106**, 215–233 (1993).
19. P. Colella and H. M. Glaz, 'Efficient solution algorithm for the Riemann problem for real gases', *J. Comput. Phys.*, **59**, 264–289 (1985).
20. J. Quirk, 'An alternative to unstructured grids for computing gas dynamic flow around arbitrarily complex two dimensional bodies', *Comput. Fluids*, **23**. 125–142 (1994).
21. R. Saurel, M. Larini and J. C. Loraud, 'Exact and approximate Riemann solvers for real gases', *J. Comput. Phys.*, **112**, 126–137 (1994).
22. A. Harten, P. D. Lax and B. van Leer, 'On upstream differencing and Godunov type schemes for hyperbolic conservation laws', *SIAM Rev.*, **25**, 33–61 (1983).
23. M. S. Liou, B. van Leer and J. S. Shuen, 'Splitting of inviscid fluxes for real gases', *J. Comput. Phys.*, **87**, 1–24 (1990).
24. S. F. Davis, 'Simplified second order Godunov type methods', *SIAM J. Sci. Statist. Comput.*, **9**, 445–473 (1988).
25. E. F. Toro, M. Spruce and W. Spearce, 'Restoration of the contact surface in the HLL-type Riemann solver', *Shock Waves*, **4**, 25–34 (1994).
26. B. Einfeld, C. D. Munz, P. L. Roe and B. Sjorgreen, 'On Godunov type methods near low densities', *J. Comput. Phys.*, **92**, 273–295 (1991).
27. G. D. Van Albada, B. van Leer and W. W. Roberts, 'A comparative study of computational methods in cosmic gas dynamics', *Astron. Astrophys.*, **108**, 76–84 (1982).
28. P. L. Roe, 'Some contribution to the modelling of discontinuous flows', *Proc. AMS/SIAM Seminar*, San Diego, CA, 1983.
29. J. Hyman, 'Numerical methods for tracking interfaces', *Physica D*, **12**, 396–407 (1984).
30. J. P. Cocchi and R. Saurel, 'A simple method for the resolution of compressible multimaterial problem', *J. Comput. Phys.*, to appear.
31. B. Bukiet, 'Application of front tracking to two dimensional curved detonation fronts', *SIAM J. Sci. Statist. Comput.*, **9**, 80–99 (1988).
32. J. Glimm, 'Solution in the large for non linear hyperbolic systems of equations', *Commun. Pure Appl. Math.*, 697–715 (1965).
33. W. Fickett and W. C. Davis, *Detonation*, University of California Press, Berkeley, CA, 1979.
34. G. Baudin, 'QUERCY, un code thermochimique adapté au calcul des caractéristiques de détonation des explosifs aluminisés', *Europyro 93, 5e Congrès Int. de Pyrotechnie*, Tours, June 1993.
35. Heuze (1989).
36. J. C. Goutelle, 'Modèles utilisés au CEG pour traiter le comportement réactif des explosifs', DGA/DRET/ETCA/CEG, Grammat, 1995 (unpublished).
37. R. F. Warming and R. W. Beam, 'Upwind second order difference schemes with applications in aerodynamic flows', *AIAA J.*, **24**, 1241–1249 (1976).

 